Publ. Astron. Soc. Japan (2014) 66 (5), 87 (1–14)
doi: 10.1093/pasj/psu063
Advance Access Publication Date: 2014 October 13

MAXI observations of gamma-ray bursts

Motoko Serino,[1,*] Takanori Sakamoto,[2] Nobuyuki Kawai,[1,3] Atsumasa Yoshida,[1,2] Masanori Ohno,[4] Yuji Ogawa,[5] Yasunori Nishimura,[5] Kosuke Fukushima,[6] Masaya Higa,[7] Kazuto Ishikawa,[3] Masaki Ishikawa,[8] Taiki Kawamuro,[9] Masashi Kimura,[10] Masaru Matsuoka,[1,10] Tatehiro Mihara,[1] Mikio Morii,[1] Yujin E. Nakagawa,[11] Satoshi Nakahira,[10] Motoki Nakajima,[12] Yuki Nakano,[2] Hitoshi Negoro,[6] Takuya Onodera,[6] Masayuki Sasaki,[13] Megumi Shidatsu,[9] Juri Sugimoto,[1] Mutsumi Sugizaki,[1] Fumitoshi Suwa,[6] Kazuhiko Suzuki,[6] Yutaro Tachibana,[3] Toshihiro Takagi,[1,6] Takahiro Toizumi,[3] Hiroshi Tomida,[10] Yohko Tsuboi,[7] Hiroshi Tsunemi,[13] Yoshihiro Ueda,[9] Shiro Ueno,[10] Ryuichi Usui,[3] Hisaki Yamada,[5] Takayuki Yamamoto,[1] Kazutaka Yamaoka,[14,15] Makoto Yamauchi,[5] Koshiro Yoshidome,[5] and Taketoshi Yoshii[3]

[1]MAXI team, Institute of Physical and Chemical Research (RIKEN), 2-1 Hirosawa, Wako, Saitama 351-0198, Japan
[2]Department of Physics and Mathematics, Aoyama Gakuin University, 5-10-1 Fuchinobe, Chuo-ku, Sagamihara, Kanagawa 252-5258, Japan
[3]Department of Physics, Tokyo Institute of Technology, 2-12-1 Ookayama, Meguro-ku, Tokyo 152-8551, Japan
[4]Department of Physical Sciences, Hiroshima University, 1-3-1 Kagamiyama, Higashi-Hiroshima, Hiroshima 739-8516, Japan
[5]Department of Applied Physics, University of Miyazaki, 1-1 Gakuen Kibanadai-nishi, Miyazaki, Miyazaki 889-2192, Japan
[6]Department of Physics, Nihon University, 1-8-14 Kanda-Surugadai, Chiyoda-ku, Tokyo 101-8308, Japan
[7]Department of Physics, Chuo University, 1-13-27 Kasuga, Bunkyo-ku, Tokyo 112-8551, Japan
[8]School of Physical Science, Space and Astronautical Science, The Graduate University for Advanced Studies, Yoshinodai 3-1-1, Chuo-ku, Sagamihara, Kanagawa 252-5210, Japan
[9]Department of Astronomy, Kyoto University, Kitashirakawa-Oiwake-cho, Sakyo-ku, Kyoto, Kyoto 606-8502, Japan
[10]ISS Science Project Office, Institute of Space and Astronautical Science (ISAS), Japan Aerospace Exploration Agency (JAXA), 2-1-1 Sengen, Tsukuba, Ibaraki 305-8505, Japan
[11]ISS Science Project Office, Institute of Space and Astronautical Science (ISAS), Japan Aerospace Exploration Agency (JAXA), 3-1-1 Yoshinodai, Chuo-ku, Sagamihara, Kanagawa 252-5210, Japan
[12]School of Dentistry at Matsudo, Nihon University, 2-870-1 Sakaecho-nishi, Matsudo, Chiba 101-8308, Japan
[13]Department of Earth and Space Science, Osaka University, 1-1 Machikaneyama, Toyonaka, Osaka 560-0043, Japan

[14]Department of Particle Physics and Astronomy, Nagoya University, Furo-cho, Chikusa-ku, Nagoya, Aichi 464-8601, Japan
[15]Solar-Terrestrial Environment Laboratory, Nagoya University, Furo-cho, Chikusa-ku, Nagoya, Aichi 464-8601, Japan

*E-mail: motoko@crab.riken.jp

Received 2014 June 13; Accepted 2014 June 13

Abstract

The Monitor of All-sky X-ray Image (MAXI) Gas Slit Camera (GSC) detects gamma-ray bursts (GRBs), including bursts with soft spectra, such as X-ray flashes (XRFs). MAXI/GSC is sensitive to the energy range from 2 to 30 keV. This energy range is lower than other currently operating instruments which are capable of detecting GRBs. Since the beginning of the MAXI operation on 2009 August 15, GSC observed 35 GRBs up to the middle of 2013. One third of them were also observed by other satellites. The rest of them show a trend to have soft spectra and low fluxes. Because of the contribution of those XRFs, the MAXI GRB rate is about three times higher than those expected from the BATSE log N–log P distribution. When we compare it to the observational results of the Wide-field X-ray Monitor on the High Energy Transient Explorer 2, which covers the the same energy range as that of MAXI/GSC, we find the possibility that many of the MAXI bursts are XRFs with $E_{\rm peak}$ lower than 20 keV. We discuss the source of soft GRBs observed only by MAXI. The MAXI log N–log S distribution suggests that the MAXI XRFs are distributed over a closer distance than hard GRBs. Since the distributions of the hardness of galactic stellar flares and X-ray bursts overlap with those of MAXI GRBs, we discuss the possibility of confusion of such galactic transients with the MAXI GRB samples.

Key words: gamma-ray burst: general — methods: data analysis — X-rays: bursts

1 Introduction

X-ray flashes (XRFs) are a subclass of gamma-ray bursts (GRBs) which have significantly softer spectra than those of classical GRBs. They are characterized by the absence of emission in the high-energy band (> 50 keV: Strohmayer et al. 1998; Heise et al. 2001). Later, the empirical classification of GRBs using fluence ratio in the 2–30 keV to 30–400 keV bands was introduced (Sakamoto et al. 2005). While the peak energy values, $E_{\rm peak}$, in the spectra of XRFs distinguish them from classical hard GRBs, Sakamoto et al. (2005) suggest that they arise from the same class based on the HETE-2 samples.

Various models have been proposed to explain the origin of low $E_{\rm peak}$ in XRFs. Some of them do not assume intrinsic difference in the source. Instead, the apparent differences from hard GRBs are caused by the redshift of the sources (Heise et al. 2001) or the observers' viewing angles of the GRB jets (Yamazaki et al. 2002). Others require an intrinsic difference in the conditions of the sources (Mészáros et al. 2002; Zhang & Mészáros 2002; Lamb et al. 2005). Some of the predictions of these models are investigated against the observed data (Granot et al. 2005; D'Alessio et al. 2006).

Although it is natural to imagine that GRBs which occurred at high redshift have low (apparent) $E_{\rm peak}$, we have not yet observed such an event. So far, all the XRFs with $E_{\rm peak}$ lower than 20 keV have relatively low redshift: the redshift values of XRF 020903 ($E_{\rm peak} < 5$ keV: Sakamoto et al. 2004), XRF 050416A ($E_{\rm peak} = 13.67$ keV: Sakamoto et al. 2006), and XRF 091018 ($E_{\rm peak} = 19.43$ keV: Sakamoto et al. 2011) are 0.25 (Soderberg et al. 2004), 0.6528 (Soderberg et al. 2007), and 0.971 (Chen et al. 2009; Wiersema et al. 2012), respectively.

There have been some attempts to estimate the luminosity function of GRBs (Butler et al. 2010; Wanderman & Piran 2010; Qin et al. 2010; Virgili et al. 2011; Lien et al. 2014). However, in order to estimate the luminosity function at high redshift more precisely, it is necessary to observe GRBs at lower energy ranges to reduce the selection effect. Monitor of All-sky X-ray Image (MAXI) is one of the X-ray instruments which have the capability of observing such an extremely soft GRB and alerting its location to the community promptly (Matsuoka et al. 2009).

MAXI is an experimental payload on the Exposed Facility of the Japanese Experiment Module attached to the International Space Station (ISS). It started nominal observation on 2009 August 15, and has been monitoring the X-ray sky since then. MAXI has two scientific instruments: the Gas Slit Camera (GSC: Mihara et al. 2011; Sugizaki et al. 2011) and the Solid-state Slit Camera (SSC: Tsunemi et al. 2010; Tomida et al. 2011). GSC has a larger effective area and field of view (FOV) than those of SSC. Therefore, GSC is suitable for detecting GRBs. In this paper, we present results based on the GSC data. The GRB observations based on SSC data will be presented elsewhere.

MAXI employs slit and collimator optics. This has an advantage over conventional coded-mask systems in reducing the contamination from the cosmic X-ray background to a point source. Therefore, MAXI GSC achieves the highest sensitivity so far as a monitoring instrument in the X-ray energy range.

One of the most comprehensive studies of GRBs below 10 keV was accomplished by Sakamoto et al. (2005). They utilized data sets observed by the Wide-field X-ray Monitor (WXM: Shirasaki et al. 2003) on the High Energy Transient Explorer 2 (HETE-2: Ricker et al. 2003). We will present here a comprehensive study of the MAXI/GSC GRB samples so that we can compare them with those of WXM.

2 Observations and data analyses

2.1 Gas Slit Camera (GSC)

The GSC consists of 12 one-dimensional position-sensitive proportional counters operating in the 2–30 keV range. Because slit and collimator optics produce a smaller FOV than coded-mask optics, the cosmic X-ray background of GSC is rather lower than HETE-2/WXM. Two GSC camera units, GSC-H (horizontal camera) and GSC-Z (zenithal camera), have an instantaneous FOV of $3^\circ \times 160^\circ$ by pointing in directions orthogonal to each other. GSC covers 70% of the whole sky every orbit.

The GSC counters are only operated within a latitude of $\pm 40^\circ$ to avoid the risk of discharge due to a high particle background that could leave damage on the carbon anode wires. Because of this restriction, the operation efficiency (i.e., fraction of actual observing time) of GSC is about 40%, except for the first 1.5 months (figure 1). The counters which experience a discharge were tentatively stopped or operated by reducing voltage from 1650 V to 1550 V—see Sugizaki et al. (2011) for details. The slight decrease of the sensitivity is expected because of the reduction of the voltage. However, we find no significant difference in the observed rate of GRBs between the periods when the cameras are operated at 1650 V and 1550 V.

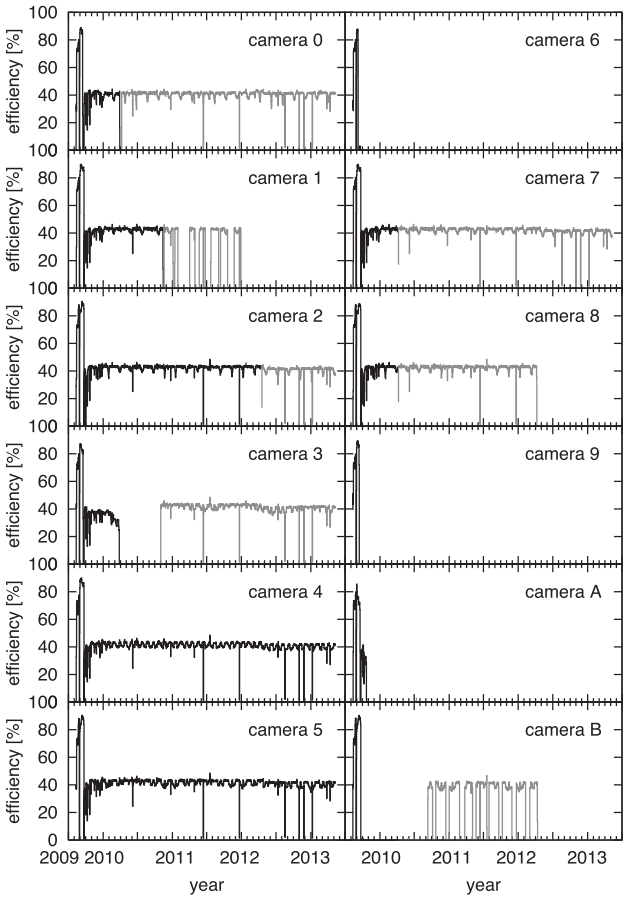

Fig. 1. The operation efficiency of GSC counters. The black and gray lines represent operation at 1650 V and 1550 V, respectively. Two cameras on the same row (e.g., camera 0 and camera 6) cover the same FOV. Loss of either one of the cameras reduces the effective area to a half.

MAXI scans a certain celestial position every 92 min—the orbital period of ISS. A typical transit time on a point source is about 40–100 s, depending on the source-acquisition angle β (Sugizaki et al. 2011). A typical effective area for a point source is about 10 cm^2 in the 4–10 keV band. In addition, the effective area presented to a source varies during a scan, because the position of the source moves in the detector plane. This variation of the effective area during a scan makes it difficult to know the intrinsic variation of a source flux. However, we can estimate the uncertainty of the average flux during a scan by the method described in sub-subsection 2.4.2.

2.2 Data reduction and sample selection

We analyzed X-ray event data of the GSC data process version 1.4. Data collected at both 1650 V and 1550 V were used in the analysis. For analyzing GRBs, we extracted X-ray events within 10° from the best burst position. All the light curves and the spectra were created from these extracted X-ray events.

There are three ways to identify GRBs or other transient events from the MAXI data. First, the transient event can be identified automatically by the search program called the MAXI Nova-Alert System (Suwa et al. 2010). Second, ground search of the MAXI data is possible by knowing the trigger time and the location of GRBs as informed by other satellites. Third, we occasionally find transient sources by eye inspection of daily or orbital all-sky images of MAXI.

We selected transient events which had a signal-to-noise ratio (S/N) larger than 5 and only lasted for one scan. If the position of the event matched within 1° a known X-ray source, we excluded it from our sample. We also excluded events which had galactic latitude b between $\pm 10^\circ$ to avoid contamination from galactic transients. The only exception is GRB 091230, which has a low galactic latitude but is confirmed as a GRB by INTEGRAL (Gotz et al. 2009).

In table 1, we describe the parameters for 35 GRBs and short X-ray transients observed by MAXI from 2009 August up to 2013 April. The columns of table 1 are as follows: "Time" is the center time of the transit in which the burst was observed. The transit time depends on the source position. If the positions of the sources are determined by X-ray or optical telescopes accurately (table 2), we used those positions; otherwise, we used the position calculated with MAXI data (subsection 2.3). "(RA, Dec)" is the GRB location calculated with MAXI data in J2000; "Localization error" is the error in the position; "Cameras" is the camera numbers which observed the GRB; "S/N" is the signal-to-noise ratio of the GRB in the 2–20 keV band; "trigger" is the method by which we found the GRB; "Other satellites" is the other satellites which observed the GRB. The trigger (or detection) time of the instrument from the time in the "Time" column are shown in square brackets. "Delay" is the time delay in sending GCN or Astronomer's Telegram after the detection of the bursts.

For the GRBs with X-ray and/or optical afterglows, we have summarized the information on the counterparts in table 2. In table 2, the "Band" column shows the band of observation of the counterparts; "(RA, Dec)" and "Error" are the GRB location in J2000.0 and its error determined by the observations of the counterparts; "GCN#" is the number of the GCN circular which reported the position of the X-ray or optical counterparts; "Redshift" is the measured redshift (and its reference) of the GRB.

2.3 Localization

A point spread function (PSF) of a constant source in the MAXI data can be represented by the product of a spatial distribution in the detector anode direction and the effective area variation in the time direction. For an instantaneous observation, a spatial distribution of the X-ray photons from a point source can be expressed as a Gaussian distribution in the MAXI data. The effective area to a source is expressed as a triangular function of the time. Therefore, a PSF of a source can be represented by the product of the Gaussian in the detector anode direction and the triangular function in the time direction.

Figure 2 shows a sample GSC PSF. An intersection of the PSF for the direction along the detector anode wire (x) is modeled with a Gaussian. An intersection of the PSF for the direction along the scan (i.e., time t) reflects the variation of the effective area during the scan, and thus has the triangular shape.

In order to determine the position of an X-ray source, first we fit the two-dimensional PSF to the position histogram of X-ray events in the x–t plane. Then the position in x–t plane is converted to celestial coordinates using the information of the ISS attitude.

During the position-fitting process, we fix the width of the Gaussian and the triangles based on the source position at the detector plane. There are three free parameters: the time at the peak, position at the detector, and normalization.

However, this PSF model is valid only for a source with constant flux. If the observed duration of the emission is significantly shorter than the transit duration (i.e., the width of the triangular function), the position in the time direction becomes ambiguous. We illustrate this situation schematically in figure 3. For the case of a long-duration event (left panels), the peak time of the triangular response can be determined without ambiguity. On the other hand, for a short event (right panels), the peak time cannot be determined as unique. We have illustrated two possible extreme cases in the panel: the burst is observed at the end (dashed line) or beginning (dash-dotted line) of the triangular response. The true response is somewhere between the two cases. This ambiguity in the peak time reflects the ambiguity in the position of the source.

In such a case, we calculate an error box of the source position based on the ambiguity in time. At first, we calculate the position assuming a constant source (i.e., fitted with the PSF for a constant source). We get a systematically small error box with this approach.

Next, we extend the error box taking into account the ambiguity in the scan (time) direction. The size of the error in this direction is $\delta\theta(T_{\rm trn} - T_{\rm d})/T_{\rm trn}$, where $\delta\theta$, $T_{\rm trn}$, and $T_{\rm d}$ are the PSF size in the scan direction, the duration of the transit, and the observed duration of the burst, respectively.

There are additional $0.^\circ 1$ systematic errors in the position determination (Morii et al. 2011).[1]

[1] When the paper was written, the systematic error was $0.^\circ 2$. After the additional position calibration, the systematic error has been reduced to $0.^\circ 1$.

Table 1. A summary of GRBs and short X-ray transients observed by MAXI.

GRB name	Time*	(RA, Dec)		Localization error†		Cameras‡	*S*/*N*	Trigger§	Other satellites‖	Delay# (hr)
090831	2009-08-31 07:37:07	145.4	+51.4	C	60′	2,8	185.3	O	F[−31](1)/K[−33](2)/W[−31](3)	12
090926B	2009-09-26 21:55:39	46.3	−39.1	C	60′	1,7	28.3	O	S[+9](4)/F[−10](5)	9
091012**	2009-10-12 10:25:51	182.82	+63.37	C	12′	0,1,7	14.6	H		
091120	2009-11-20 04:35:20	226.81	−21.79	C	30′	1,7	272.1	O	F[−40](6)/K[−44](7)	97
091201	2009-12-01 21:48:36	118.6	+16.6	C	24′	3	19.0	M		19
091230**	2009-12-30 06:27:15	132.91	−53.88	C	21′	2,8	9.2	O	I[+15](8)	
100315A	2010-03-15 17:13:40	74.95	−6.63	B	166′ × 45′	2,8	8.0	M		14
100327	2010-03-27 17:08:20	346.03	+42.90	B	58′ × 28′	1,7	12.4	M		66
100415A	2010-04-15 03:44:54	7.48	−15.57	B	104′ × 36′	4	26.6	M		9
100510A	2010-05-10 19:27:23	355.8	−35.6	B	83′ × 16′	1	51.2	M	F[−16](9)	24
100616A	2010-06-16 01:42:17	50.95	−40.62	B	110′ × 70′	4,5	14.0	M		8
100701A	2010-07-01 06:54:31	188.86	−34.26	B	122′ × 21′	5	32.5	M		5
100823A	2010-08-23 17:25:52	20.70	+5.84	C	7′	4,5	67.4	O	S[−17](10)	95
100911	2010-09-11 14:58:24	103.41	−70.43	B	39′ × 15′	1,2	8.7	H		41
101117A	2010-11-17 07:32:57	89.63	−2.30	B	38′ × 22′	0	28.4	M		3
101210**	2010-12-10 03:38:27	61.66	−5.36	C	20′	4,5,B	8.8	M		
110213B	2011-02-13 14:32:08	41.76	+1.15	B	40′ × 7′	4	139.8	M	K[−35](11)	14
110402**	2010-04-02 02:33:55	62.52	−3.00	E	30′ × 20′	0,7	11.6	M		
110426A	2011-04-26 15:08:35	221.18	−10.78	B	262′ × 16′	4,5	20.2	M	F[−128](12)	9
110916	2011-09-16 20:33:12	171.68	−17.77	B	77′ × 19′	2,8	13.8	M		85
111024A	2011-10-24 07:21:44	221.93	+25.87	B	12′ × 9′	4	74.8	M		5
120424A	2012-04-24 16:47:29	23.985	−29.87	C	16′	4,5	17.1	M		19
120510A	2012-05-10 08:48:06	44.285	+72.850	C	10′	0,7	52.8	M	K(13)††	5
120528B	2012-05-28 18:12:08	77.59	−37.80	B	78′ × 22′	2,7	26.5	M	K[−20](14)	8
120528C	2012-05-28 21:20:45	12.93	−0.95	E	48′ × 36′	4,5	6.9	H		31
120614A	2012-06-14 05:49:10	312.73	+65.16	C	10′	0,7	33.2	M		2
120622A	2012-06-22 03:21:51	205.43	−1.71	B	130′ × 30′	2	12.1	M		2
120626B	2012-06-26 13:38:12	175.77	+68.50	C	30′	0,7	10.5	M		44
120711A	2012-07-11 02:45:07	94.703	−71.001	B	65′ × 13′	2	21.4	M	F[−14](15)/L(16)/I[−19](17)/K[+49](18)	8
120908A	2012-09-08 22:35:12	230.64	−25.79	E	28′ × 19′	4,5	6.2	M	F[−252](19)	11
121025A	2012-10-25 07:46:30	248.75	+27.73	C	17′	4,5	7.0	M		3
121209A	2012-12-09 21:59:08	327.02	−7.69	C	24′	4,5	9.4	O	S[+3](20)	111
121229A	2012-12-29 05:01:09	190.10	−50.59	C	24′	2,7	12.2	O	S[−48](21)	4
130102B	2013-01-02 04:42:03	309.58	−72.38	C	12′	2	35.3	M	K(22)††	25
130407A	2013-04-07 23:36:57	248.10	+10.51	C	12′	4,5	14.9	M		4

*The center time of the transit in which the burst was observed.

†The size of localization error in arcmin. C, B, and E denote the shape of the error—C: circle (radius), B: rectangular box (length), and E: ellipsoid (long and short radii), respectively. The systematic errors are not included.

‡Camera IDs of the cameras that observed the burst. There are 12 cameras: camera 0–9, camera A, and camera B.

§M, O, and H denote that they are found by the MAXI Nova-Alert System, information from other satellites, and human inspection, respectively.

‖F: Fermi/GBM, L: Fermi/LAT, S: Swift, I: INTEGRAL, K: Konus-Wind, W: Suzaku/WAM. The numbers in the square brackets are the trigger (or detection) time of the instrument from the time in the "Time" column. The reference numbers are in parentheses. The references are as follows: (1) Rau (2009); (2) Golenetskii et al. (2009b); (3) Ohmori et al. (2009); (4) Grupe et al. (2009); (5) Briggs (2009); (6) Gruber (2009); (7) Golenetskii et al. (2009a); (8) Gotz et al. (2009); (9) Bhat et al. (2010); (10) Mangano et al. (2010); (11) Golenetskii et al. (2011); (12) van der Horst & Camero-Arranz (2011); (13) Golenetskii et al. (2012b); (14) Golenetskii et al. (2012c); (15) Gruber and Pelassa (2012); (16) Tam, Li, and Kong (2012); (17) Gotz et al. (2012); (18) Golenetskii et al. (2012a); (19) McGlynn (2012); (20) Maselli et al. (2012); (21) Sonbas et al. (2012); (22) Golenetskii et al. (2013).

#The time delay in sending GCN or Astronomer's Telegram.

**Not reported to GCN or Astronomer's Telegram.

††The detection time is not reported.

Table 2. X-ray and optical counterparts of MAXI GRBs.

GRB name	Band	(RA, Dec)		Error	GCN#*	Redshift (ref.)†
090926B	optical	46.30808	−39.00617	0.″5	9944	1.24 (1)
091230	optical	132.91325	−53.89797	0.″5	10299	
100823A	optical	20.70429	+5.83511	0.″9	11148	
110213B	optical	41.75588	+1.14619		11732	1.083 (2)
120510A	X-ray(?)‡	44.04666	+72.88692	4.″8	13284	
120711A	optical	94.67850	−70.99911		13430	1.405 (3)
121025A	X-ray	248.38182	+27.67189	3.″8	13909	
121209A	optical	326.78733	−8.23508	0.″5	14049	2.707 (4)
121229A	optical	190.10121	−50.59430	0.″5	14117	

*The number of the GCN circular which reported the position of the X-ray or optical counterparts.

†The references are (1) Fynbo et al. (2009); (2) Cenko et al. (2011); (3) Tanvir et al. (2012); (4) Fynbo et al. (2012).

‡A candidate afterglow was reported, but not confirmed.

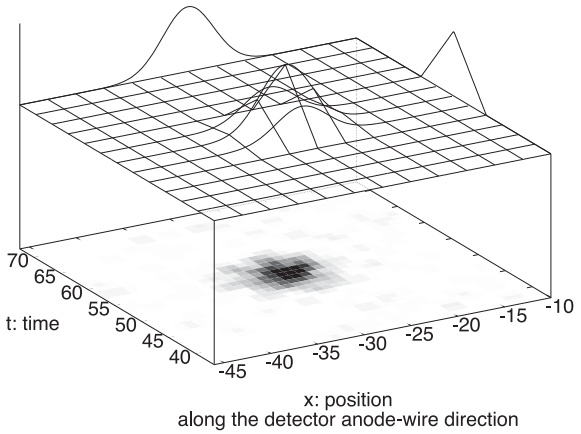

Fig. 2. A schematic view of the PSF fit of an X-ray source. The bottom map is the observed X-ray image of an X-ray source. We fitted the PSF (the above function) to the image. An intersection of the PSF for the direction along the detector anode wire (x) is modeled with a Gaussian. The triangular shape of an intersection of the PSF for the direction along the scan (i.e., time t) reflects the variation of the effective area during the scan. The shapes of the intersections are also shown in the figure. The free parameters in fitting are position of the peak in the x–t plane, which corresponds to the position in celestial coordinates, and the normalization, which corresponds to the source flux.

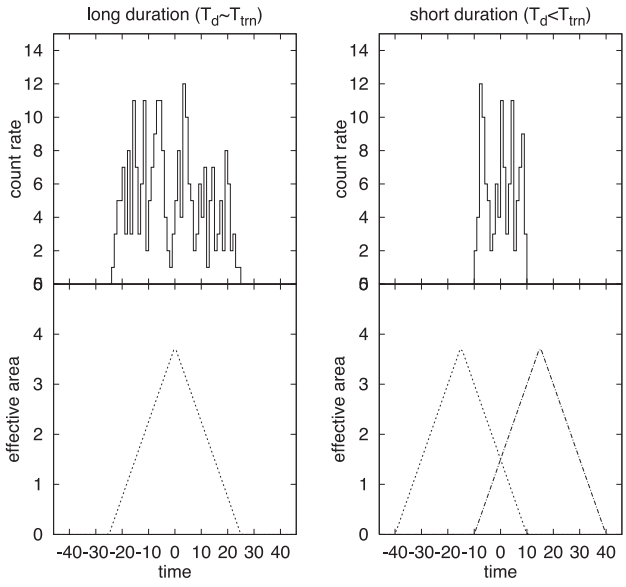

Fig. 3. Illustrations of localization ambiguity for long-duration (left) and short-duration (right) events. The solid lines are the simulated observed count rate curves and the dashed lines or the dash-dotted lines are the effective area curves. When the event duration is short, the source position (time) cannot be determined as unique.

Figure 4 shows an example of localization error circles and boxes for GRB 110213B. The small solid error box is the result of a fit under the assumption of the PSF of a constant source. If we consider the shortness of the detection time, the error box is extended toward the direction of the scan, resulting in the dashed box.

The position determined only by the MAXI data is entirely consistent with the optical counterpart position by taking into account the systematic error. Figure 5 shows the all-sky map of the MAXI GRBs.

2.4 Light curves of the bursts

2.4.1 Light curves of MAXI bursts

To create light curves of MAXI bursts, we have to select the source region in the image. In order to reduce systematic background variation, we adopted data selection using detector coordinates, rather than celestial coordinates. We selected the region where the separation of the source-acquisition angle, which is the angle with respect to the orbital plane of MAXI (Mihara et al. 2011), from the position of the source is $|\delta\beta| \leq 1.^{\circ}5$. The selected region

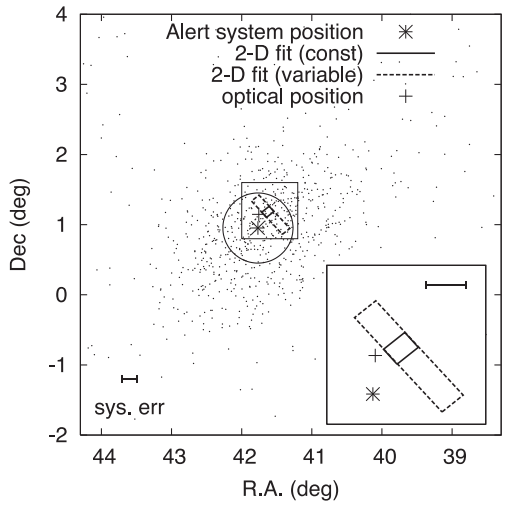

Fig. 4. The localization error boxes of GRB 110213B. The dots are the positions of the X-ray events in celestial coordinates. The star mark and the circle show the position and the error circle derived by the MAXI Nova-Alert System, respectively. The solid and dashed boxes represent the positions derived by two-dimensional source fitting, where constant and variable flux of the source are assumed, respectively. The horizontal bars indicate the magnitude of the systematic error for these error boxes. The position of the optical counterpart of this GRB is shown with the plus mark. The square region is expanded in the inset.

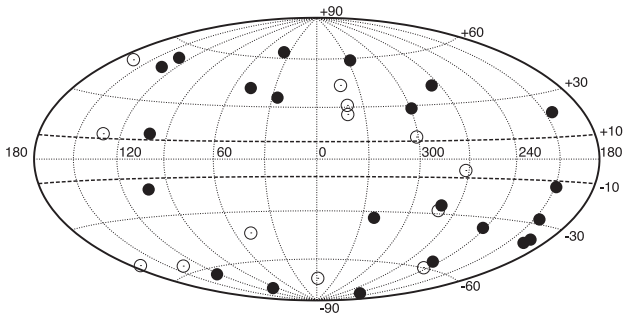

Fig. 5. An all-sky map of MAXI GRBs in galactic coordinates. The open circles are the positions of the GRBs also observed by other satellites. The filled circles are the positions of the GRBs observed only by MAXI. The thick dashed lines are at the galactic latitude $b = \pm 10^\circ$, where we excluded events (see text for details).

projected to celestial coordinates forms a belt-like region with a width of 3°.

The light curves of MAXI data are as a result of a convolution of the source variation and a change of the effective area. In order to see the intrinsic source variation, we divide the observed counts by the effective area at the time. However, if the duration of an event is shorter than the transit time, the position of a source cannot be determined, as mentioned in the previous section. In such a case, the effective area and the flux variation of the source may also be ambiguous.

The left panels of figure 6 show samples of light curves of GRB 091120 observed by MAXI, compared with those of Fermi/GBM (Meegan et al. 2009). According to the light curves of Fermi/GBM, the duration of this burst is much longer than the transit time. Therefore the localization error is relatively small. We corrected the MAXI light curves with the effective area of each energy band. Note that we assumed a photon index of −2 when we calculate the effective area. The right panels of figure 6 show the light curves of GRB 111024A, which is not observed by other satellites. The light curves are variable, like classical GRBs. However, most of the MAXI bursts are not bright enough to observe the variability. The light curves of all MAXI bursts presented in this paper are available on the MAXI web page.[2]

2.4.2 Hardness and intensity analyses

Because the effective area of GSC can only achieve typically $\sim 10\,\mathrm{cm}^2$, GSC usually does not have enough photons to perform spectral analysis for short-lived events. Therefore we decided to study two parameters, the average energy flux and the hardness ratio, which can be derived without performing spectral analysis with a relatively small assumption.

The hardness ratio is defined as the ratio of the photon flux in the 8–20 keV band to that in the 2–8 keV band, assuming a spectral slope of −2.[3] In order to calculate the average flux in units of $\mathrm{erg\,cm^{-2}\,s^{-1}}$, first we calculated the average photon flux in the 2–20 keV band. The average photon flux is determined as the total counts of the bursts in the 2–20 keV band divided by the total effective area times the scan duration around the burst. The background count rate is calculated from the count rate before and after the transit. After the background subtraction, the total count for the burst is calculated as the observed count during the transit.

To obtain a reliable energy flux, we took into account the spectral hardness of the burst in calculating the effective area. We calculated a photon index in the simple power-law model from the observed hardness ratio. Then the photon flux is converted into the energy flux using this estimated photon index.

The uncertainty in the flux measurement comes not only from statistical error but also from systematic uncertainty of the effective area. The degree of this systematic uncertainty depends on the ratio of the observed duration of the burst T_d to the duration of the transit T_trn. Since MAXI may not observe a whole GRB, T_d does not mean usual "duration" (like T_{90}), but it means the lower limit of the duration. In the case of $T_\mathrm{d}/T_\mathrm{trn} \geq 0.5$, the maximum uncertainty is

[2] ⟨http://maxi.riken.jp/grbs⟩.

[3] We re-calculate the hardness using the spectral slope estimated from the hardness. However, the change due to the assumed spectral slope is smaller than the statistical error of the hardness.

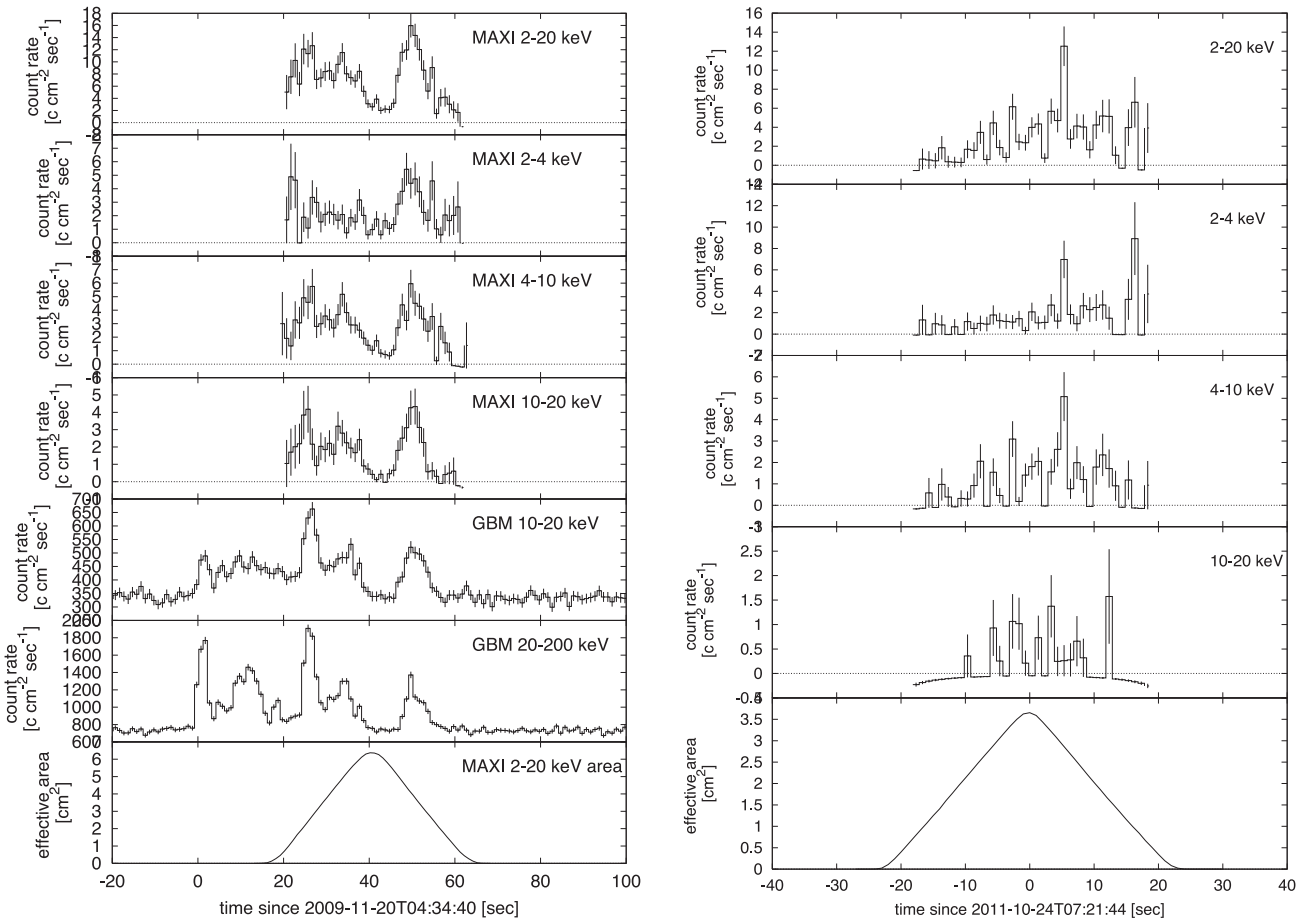

Fig. 6. Light curves of GRB 091120 (left) and GRB 111024A (right). The light curves of MAXI are corrected with the effective area of each energy band. For GRB 091120, the light curves observed by Fermi/GBM are also plotted for comparison. Effective area curves are shown in the bottom panels.

1.5 (i.e., the flux is underestimated and the true flux can be 1.5 times higher than that calculated from the MAXI data). If $T_{\rm d}/T_{\rm trn} < 0.5$, the maximum uncertainty in flux can be expressed as

$$\frac{T_{\rm trn}}{T_{\rm d}} - \frac{1}{2}, \tag{1}$$

which becomes larger for a shorter burst.

In addition, there is the possibility that the average flux here is different from the average flux observed by other satellites. This is because MAXI may observe only a part of a long GRB. In fact, GRB 120711 became five times brighter than the flux at the time of the MAXI observation after the end of MAXI transit. So, the average flux here should be treated with care.

The flux and hardness parameters are summarized in table 3. Figure 7 shows the relationship between the hardness ratio and the time-averaged flux. The bursts observed only by MAXI ("only MAXI," triangles) tend to distribute at the soft and the low flux region (the lower-left part of the plot). On the other hand, most of the bright ($> 10^{-8}$ erg cm^{-2} s^{-1}) bursts, which were also observed by other instruments simultaneously ("simul.-GRBs," circles), show relatively hard spectra. From this figure, we conclude that MAXI/GSC is generally sensitive to soft and dim bursts. Averages of the hardness of "only MAXI" and "simul.-GRBs" are 0.32 and 0.54, respectively.

2.5 Spectral analyses

We selected bright GRBs with high S/N (> 35) to have enough statistics to perform spectral analysis. There are seven GRBs that satisfy this criterion. If the bursts were simultaneously observed by Swift/BAT (Barthelmy et al. 2005) or Fermi/GBM (Meegan et al. 2009), we performed a joint spectral fit of the MAXI spectrum and the spectrum of those instruments. The spectrum of those high-energy instruments is useful to constrain the broad-band spectral shape of GRBs. Since the MAXI transit time is rather short, the entire GRB episode can extend beyond the transit time. In these cases, we truncated the data of other missions into the same start and end time as MAXI's transit time for the spectral analyses.

Table 3. A summary of the flux and the spectral hardness.

GRB name	Flux*	Hardness†	T_d‡	Other sat.§
090831	$4.91 \pm 0.14 + 2.68$	0.47 ± 0.04	41.0	yes
090926B	1.68 ± 0.15 —	1.75 ± 0.47	21.3	yes
091012	$0.38 \pm 0.04 + 0.01$	0.32 ± 0.09	43.4	
091120	$7.69 \pm 0.23 + 2.54$	0.46 ± 0.04	29.4	yes
091201	$0.47 \pm 0.06 + 0.12$	0.34 ± 0.14	42.0	
091230	0.27 ± 0.04 —	1.06 ± 0.38	54.7	yes
100315A	$0.17 \pm 0.03 + 0.27$	0.25 ± 0.13	26.8	
100327	$0.26 \pm 0.03 + 0.03$	0.20 ± 0.09	34.6	
100415A	$0.96 \pm 0.11 + 0.57$	0.38 ± 0.13	23.4	
100510A	$2.57 \pm 0.19 + 0.75$	0.54 ± 0.11	28.0	yes
100616A	$0.37 \pm 0.05 + 0.03$	0.44 ± 0.16	38.7	
100701A	$0.88 \pm 0.09 + 1.62$	0.11 ± 0.04	19.8	
100823A	1.90 ± 0.10 —	0.24 ± 0.04	22.9	yes
100911	$0.30 \pm 0.03 + 0.02$	0.40 ± 0.13	37.4	
101117A	$0.84 \pm 0.09 + 0.73$	0.28 ± 0.09	30.0	
101210	$0.22 \pm 0.03 + 0.03$	0.48 ± 0.20	33.5	
110213B	7.58 ± 0.32 —	0.43 ± 0.05	28.4	yes
110402	$0.44 \pm 0.05 + 0.00$	0.33 ± 0.11	53.0	
110426A	$0.51 \pm 0.06 + 0.79$	0.21 ± 0.08	17.3	yes
110916	$0.27 \pm 0.03 + 0.17$	0.12 ± 0.05	43.7	
111024A	$2.76 \pm 0.17 + 1.48$	0.19 ± 0.04	23.6	
120424A	$0.47 \pm 0.05 + 0.08$	0.22 ± 0.07	32.9	
120510A	1.53 ± 0.12 —	0.52 ± 0.12	18.8	yes
120528B	$1.28 \pm 0.10 + 0.80$	0.39 ± 0.09	23.5	yes
120528C	$0.32 \pm 0.05 + 0.04$	1.17 ± 0.53	36.0	
120614A	$0.96 \pm 0.07 + 0.36$	0.30 ± 0.07	29.5	
120622A	$0.45 \pm 0.06 + 0.21$	0.22 ± 0.10	36.0	
120626B	$0.31 \pm 0.04 + 0.20$	0.27 ± 0.12	23.7	
120711A	0.99 ± 0.10 —	0.42 ± 0.12	46.7	yes
120908A	$0.18 \pm 0.03 + 0.04$	0.23 ± 0.12	33.1	yes
121025A	0.33 ± 0.06 —	0.22 ± 0.13	14.6	
121209A	0.52 ± 0.06 —	0.86 ± 0.30	59.0	yes
121229A	0.42 ± 0.05 —	0.21 ± 0.08	32.7	yes
130102B	$1.36 \pm 0.11 + 0.49$	0.35 ± 0.08	44.0	yes
130407A	$0.41 \pm 0.05 + 0.46$	0.26 ± 0.10	19.5	

*In units of 10^{-8} erg cm^{-2} s^{-1} in 2–20 keV. The first error is the statistical error and the second error is the systematic error due to the uncertainty in the effective area. For a burst with accurate position, the systematic error is negligible.

†Ratio of the photon flux in 8–20 keV to 2–8 keV.

‡The observed duration, which means the lower limit of the real duration of the burst, in seconds.

§Bursts also observed by other satellites are indicated.

We analyzed the time-averaged spectra of seven GRBs. Four of them are jointly fitted with GBM or BAT data. We tested three types of model: power-law (PL), power-law with exponential cutoff (CPL), and GRB model (GRBM) (the so-called Band function: Band et al. 1993). In performing the spectral analyses without GBM or BAT data, the $E_{\rm peak}$ may converge at an inappropriate value due to the limitation of the GSC energy range. In such a case, we calculated a lower limit of $E_{\rm peak}$ at 90% confidence by fixing the low-energy photon index α to -1.0. When the high-energy photon index β is not well constrained, we fix the index β to -2.3. We do not consider these models with artificially fixed parameters as the best-fit models. The results are summarized in table 4. All the errors in the table are 90% confidence. Although the S/N of GRB 090926B is lower than our criteria, we also listed the spectral parameters of GRB 090926B in the table, because they are already given by Serino et al. (2011). The $E_{\rm peak}$ of the MAXI–Fermi GRBs are in the 60–100 keV range, while the $E_{\rm peak}$ of the MAXI–Swift and MAXI GRBs may be located below 20 keV.

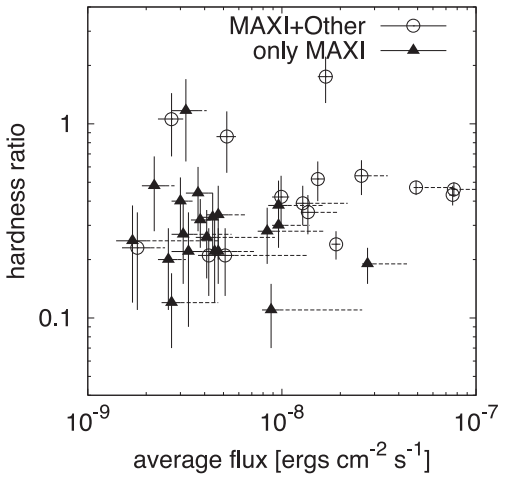

Fig. 7. Flux and hardness of MAXI GRBs. The bursts which were also observed by other instruments are plotted with circles ("simul.-GRBs"). The bursts which were not observed by other instruments are plotted with triangles. The solid error bars correspond to the statistic errors and the dashed error bars on the average flux correspond to the systematic errors.

3 Discussions

3.1 GRB rate and detection sensitivity

Conventional studies of GRB rate are targeted on relatively high energy bands. For example, Stern, Atteia, and Hurley (2002) made a log N–log P curve in the 50–300 keV band using BATSE and Ulysses samples. Suzuki and the MAXI Team (2009) estimated that the detection limit of MAXI/GSC is equivalent to 0.4 photons cm^{-2} s^{-1} in the 50–300 keV band based on a simulation study. The corresponding rate is about 400 GRBs per year. An average observing efficiency of MAXI/GSC is about 40% and sky coverage is about 2% of the whole sky. Multiplying these numbers, we expect ~ 3 events per year for the MAXI GRB rate. However, we have observed 35 events in 44 months, which is more than three times higher than this estimation. Interestingly, the rate of "simul.-GRB" is close to the expected rate. Since two thirds of MAXI GRBs are probably not observed by other satellites, those MAXI GRBs are not included in the calculation of the expected number by Suzuki and the MAXI Team (2009). According to figure 7, most of GRBs of hardness > 0.4 are "simul.-GRB." On the other hand, "only MAXI" bursts dominate the range of

Table 4. A summary of the spectral parameters and the flux.

GRB name	Joint	Model	α	β	$E_{\rm peak}$	Flux*	χ^2(DoF)
090831	Fermi	PL	$-1.62^{+0.02}_{-0.02}$	—	—	$(3.95^{+0.12}_{-0.11})$	456.23 (261)
		CPL	$-1.27^{+0.04}_{-0.04}$	—	161^{+27}_{-20}	$4.73^{+0.15}_{-0.19}$	349.23 (260)
		GRBM†	$-1.03^{+0.11}_{-0.08}$	$-1.78^{+0.06}_{-0.06}$	60^{+16}_{-15}	$5.06^{+0.10}_{-0.25}$	312.60 (259)
090926B‡	Fermi	CPL	$0.44^{+0.14}_{-0.13}$	—	97^{+7}_{-6}	$1.60^{+0.04}_{-0.03}$	93.26 (83)
		GRBM†	$0.65^{+0.22}_{-0.18}$	$-2.51^{+0.29}_{-0.49}$	85^{+9}_{-9}	$1.62^{+0.13}_{-0.18}$	83.13 (82)
091120	Fermi	PL	-1.56§	—	—	(7.60‡)	417.23 (76)
		CPL†	$-1.15^{+0.06}_{-0.05}$	—	90^{+9}_{-7}	$5.72^{+0.19}_{-0.22}$	126.71 (75)
		GRBM	$-1.14^{-0.06}_{-0.06}$	-2.3 (fixed)	83^{+10}_{-9}	$7.23^{+0.32}_{-0.22}$	135.74 (75)
100510A	Fermi	PL	$-1.58^{+0.04}_{-0.05}$	—	—	$2.54^{+0.24}_{-0.24}$	85.15 (48)
		CPL†	$-1.19^{+0.14}_{-0.13}$	—	82^{+26}_{-16}	$2.51^{+0.24}_{-0.29}$	46.87 (47)
		GRBM	$-1.19^{+0.16}_{-0.13}$	-2.3 (fixed)	78^{+29}_{-20}	$2.52^{+0.44}_{-0.24}$	48.27 (47)
100823A	Swift	PL	$-2.06^{+0.06}_{-0.06}$	—	—	$1.99^{+0.15}_{-0.13}$	53.88 (51)
		CPL†	$-1.95^{+0.15}_{-0.05}$	—	8^{+10}_{-8}	$2.02^{+0.15}_{-0.17}$	51.58 (50)
		GRBM	$-1.88^{+0.36}_{-0.23}$	-2.3 (fixed)	10^{+7}_{-9}	$2.04^{+2.13}_{-2.00}$	50.95 (50)
110213B	NA	PL	$-1.17^{+0.10}_{-0.10}$	—	—	$8.12^{+0.63}_{-0.56}$	22.77 (21)
		CPL†	$-0.53^{+0.44}_{-0.39}$	—	18^{+17}_{-5}	$8.34^{+0.17}_{-5.25}$	14.49 (20)
111024A	NA	PL†	$-2.14^{+0.18}_{-0.20}$	—	—	$3.11^{+0.34}_{-0.33}$	18.71 (21)
		CPL	-1.00 (fixed)	—	>4	$2.95^{+0.31}_{-0.53}$	16.86 (21)
120510A	NA	PL†	$-1.30^{+0.25}_{-0.27}$	—	—	$1.20^{+0.24}_{-0.20}$	15.43 (18)
		CPL	-1.00 (fixed)	—	>12	$1.19^{+0.18}_{-1.19}$	14.04 (18)

*in units of 10^{-8} erg cm^{-2} s^{-1} in 2–20 keV.
†The best-fit models for each burst are marked.
†The parameters are from Serino et al. (2011).
§The errors are not available.

hardness < 0.4 and also tend to be underluminous. Therefore, it is reasonable that the GRB rate expected from log N–log P based on BATSE and Ulysses samples does not agree with the observed rate in the MAXI/GSC energy band. This fact suggests that many soft bursts failed to be detected by the traditional GRB instruments.

There is convincing evidence of the existence of soft and underluminous GRBs. According to Meegan et al. (2009), Fermi/GBM operates 90% of the time. About 50% of MAXI events are occulted by the Earth for Fermi/GBM. We confirmed that 17 out of 35 MAXI GRBs were inside the Fermi/GBM FOV and not occulted by the Earth. However, only seven GRBs were detected by Fermi/GBM. Thus, for the other 10 events, we analyzed the daily monitoring CSPEC data, which are publicly available on the Fermi Science Support Center web page.[4] We cannot find any significant signal around the MAXI trigger time for all those 10 events. Figure 8 shows the flux and hardness of the GRBs with or without Fermi/GBM detection. GRB 110426A and GRB 120908A, plotted with triangles, were also triggered by GBM, but the trigger times were before the MAXI observations (cf. table 1). At the time of the MAXI observation,

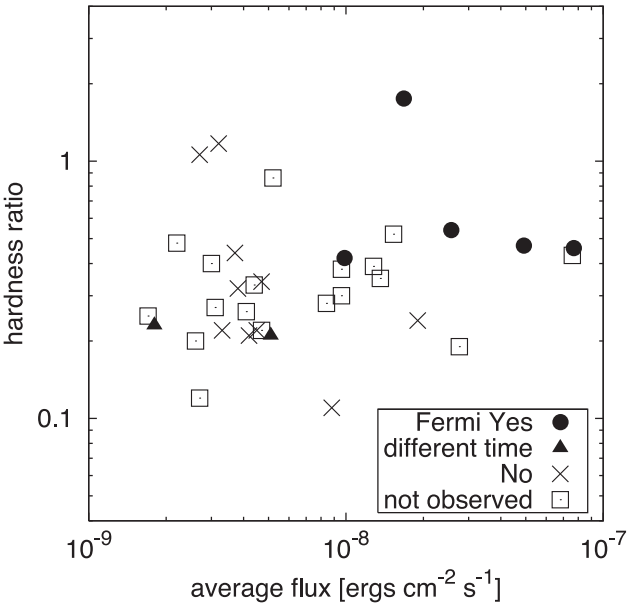

Fig. 8. Flux and hardness of MAXI GRBs with or without Fermi/GBM detection. The bursts which are also observed by GBM are plotted with circles. Two events shown by triangles were detected by GBM, but the trigger times were not during the MAXI transit (see text). The bursts shown with cross marks were observed but no significant signal was found. The bursts shown with squares were not observed (occulted or occurred during the off time) by GBM.

[4] ⟨http://fermi.gsfc.nasa.gov/ssc/⟩.

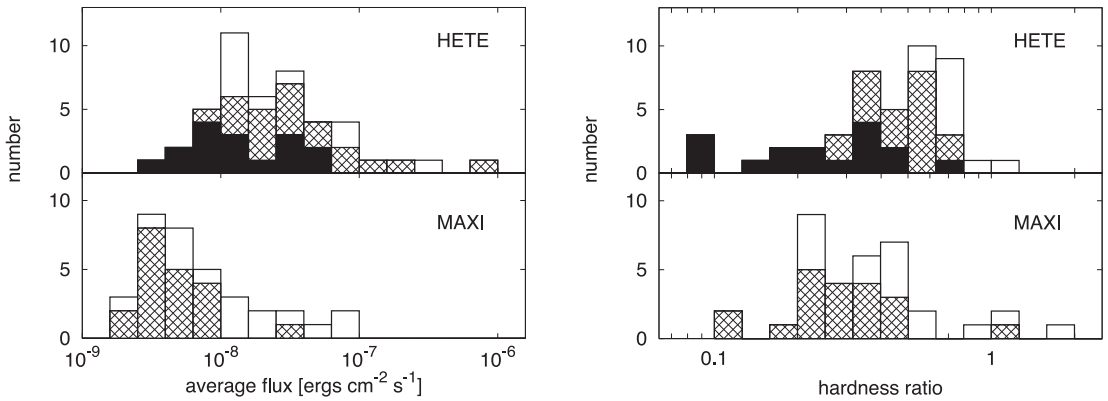

Fig. 9. Histograms of time-averaged flux in the 2–20 keV band (left) and hardness distribution (right) of MAXI and HETE-2 GRBs. The hardness is defined as the ratio of photon flux in the 8–20 keV band to the 2–8 keV band. The histograms in the top panels are results from HETE-2/WXM (Sakamoto et al. 2005). The histograms for MAXI/GSC are plotted in the bottom panels. The GRBs observed by HETE-2 are classified into (classical) GRBs (open), X-ray-rich GRBs (hatched), and X-ray flashes (filled). The hatched bursts in the bottom panels are "only MAXI" bursts.

the signal in the GBM data is not apparent. There is a clear trend in the figure. Fermi/GBM detected bright and hard events among the MAXI GRBs.

GRB 101117A was in the FOV of Swift/BAT, but no significant signal was seen in the BAT data. For Suzaku/WAM (Yamaoka et al. 2009), only GRB 090831 was detected. Of the other 34 GRBs, 19 were not occulted by the Earth nor occurred during the off time. Based on those studies, we concluded that a large fraction of MAXI GRBs are not detectable by the traditional GRB instruments.

In order to compare the results with observations in a similar energy range, we plotted histograms of flux and hardness distribution of GRBs observed by HETE-2/WXM (Sakamoto et al. 2005) in figure 9. From the left panel, we see that the average flux of the MAXI bursts are systematically lower than those of the WXM GRBs. Although the effective area of GSC is 3–6 times smaller than that of WXM, the slit and collimator optics of GSC make the background lower and thus achieves higher sensitivity than WXM. The right panels of figure 9 show the distribution of the hardness of the MAXI and the HETE samples. The hardness distribution of the MAXI GRBs, especially "only MAXI" bursts, has a similar trend to that of the HETE XRFs. We can compare the mean hardness value of each GRB class: The HETE XRFs, X-ray-rich GRBs, and classical GRBs have a mean hardness of 0.29, 0.49, and 0.75, respectively. The mean hardness of "only MAXI" bursts is 0.32, and it is nearest to the HETE XRFs.

3.2 Spectral properties of MAXI bursts

MAXI has a unique capability to observe soft GRBs. In HETE-2 samples, about one third of GRBs are classified into XRFs (Sakamoto et al. 2005). Although it is difficult to classify GRBs solely from the MAXI data, we expect that roughly one third of the MAXI GRBs are classified into XRFs on the basis of the similarity between the distributions of the hardness of MAXI and HETE bursts.

A traditional parameter, $E_{\rm peak}$, is used to represent the softness of GRBs. However, only a few bursts have enough statistics for spectral analysis in the MAXI samples. Instead of $E_{\rm peak}$ we calculated the hardness of the bursts (subsubsection 2.4.2). In order to examine the relationship between $E_{\rm peak}$ and the hardness, we calculated the hardness ratio in the MAXI energy bands, the photon flux in the 8–20 keV band to the 2–8 keV band, using the Band function with fixed indices $\alpha = -1.0$ and $\beta = -2.3$. The result is shown in figure 10. According to Kaneko et al. (2006), the distributions of indices α and β have a deviation of ~ 0.3. Considering this deviation, we also plotted the curves of a harder ($\alpha = -0.7$, $\beta = -2.0$) and a softer ($\alpha = -1.3$, $\beta = -2.6$) case in dashed lines. In this figure, we also plotted the best-fit $E_{\rm peak}$ or its lower limits for the eight MAXI GRBs shown in table 4. Although the uncertainties of the $E_{\rm peak}$ obtained from the spectral analyses are large, they are consistent with the $E_{\rm peak}$ inferred from the hardness. The exception is GRB 090926B, located far to the right with hardness >1. Since the spectral index α of this burst is positive (Serino et al. 2011) and far from the assumed value of -1, it is not surprising that this GRB does not follow the relationship.

In figure 9, we see most of the "only MAXI" events have hardness < 0.4. According to figure 10, a hardness of < 0.4 corresponds to $E_{\rm peak} < 20$ keV. Since all the bursts which have $E_{\rm peak} < 20$ are classified as XRFs (Sakamoto et al. 2005, 2008), most of the "only MAXI" events can be classified as XRFs.

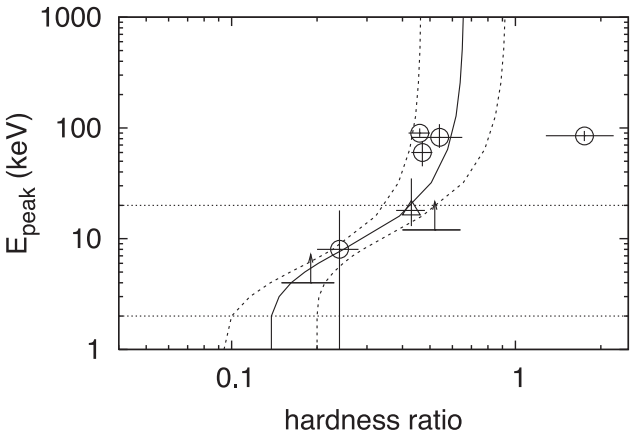

Fig. 10. The relation between hardness ratio (8–20 keV/2–8 keV) and E_{peak} for MAXI GRBs. The solid line shows the correlation calculated with the Band function with spectral indices $\alpha = -1.0$ and $\beta = -2.3$. The right and left dashed curves correspond to a harder ($\alpha = -0.7$, $\beta = -2.0$) or a softer ($\alpha = -1.3$, $\beta = -2.6$) spectral model, respectively. The open circles are results from the joint spectral fitting with other instruments. GRB 110213B is plotted with the triangle. For GRB 111024A and GRB 120510A, we cannot obtain reasonable E_{peak} without fixing α. Therefore, lower limits calculated with fixed $\alpha = -1$ are shown with arrows. The horizontal dotted lines show the upper and lower boundaries of the GSC energy range used for the hardness calculation.

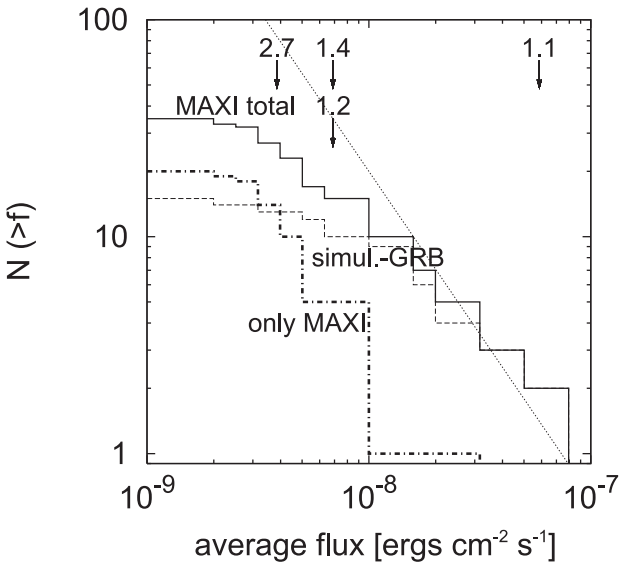

Fig. 11. The cumulative distribution of average flux. The solid, dashed, and dash-dotted lines represent the numbers of total, "simul.-GRBs," and "only MAXI" events, respectively. The dotted line has a slope of $-3/2$, indicating a uniform distribution. The arrows show the fluxes of four GRBs with known redshifts; the numbers on the arrows are their redshift values.

3.3 What does MAXI observe?

An essential question is whether the "only MAXI" events are XRFs or other transient phenomena. A reliable way to answer the question is to carry out follow-up observations of these bursts at other wavelengths. However, we have not succeeded in this yet. We do not know the redshift for any of the "only MAXI" events so far.

Instead of direct study of the distribution of distance to the source, we plotted the cumulative distribution of the average flux in figure 11. In the figure, we also indicated the fluxes of four bursts with known redshifts, which are "simul.-GRBs." The best-fit slope to the observed distribution of "simul.-GRBs" becomes flatter than $-3/2$ below a flux of around 10^{-8} erg cm^{-2} s^{-1}, while the slope of "only MAXI" bursts is close to $-3/2$ down to a flux range of 3×10^{-9} erg cm^{-2} s^{-1}. This would suggest that "only MAXI" bursts have a uniform distribution down to 3×10^{-9} erg cm^{-2} s^{-1} and that there is no selection effect of the triggering sensitivity above this level. Generally the flattening of the slope from $-3/2$ at the low flux is interpreted as a cosmological effect (Meegan et al. 1992). Therefore the difference in the slope of "only MAXI" GRBs suggests an intrinsically different population from "simul.-GRBs." The "only MAXI" GRBs have low luminosity and are distributed closer to us than the "simul.-GRBs." Sakamoto (2004) inferred that XRFs observed by HETE-2 are distributed at closer distances than hard GRBs, because the slope of the HETE-2 $\log N$–$\log P$ distribution for XRFs is steeper than that of hard GRBs above 2 photons cm^{-2} s^{-1}. Our MAXI result shows a trend similar to the results of HETE-2.

Is there any possibility that "only MAXI" events are galactic transients? In order to investigate whether we can distinguish galactic transients from GRBs by hardness ratio or not, we calculated the hardness of galactic transients. As sources of galactic transients, we considered (type-I) X-ray bursts (XRBs), which are thermonuclear flashes on neutron stars, and stellar flares. We plotted the distribution of hardness of GRBs and galactic transients in figure 12. The hardness range of GRBs overlaps with those of XRBs or stellar flares. Therefore it is difficult to distinguish between GRBs and XRBs only from the hardness ratio. The most reliable way to distinguish GRBs from XRBs or stellar flares is to refer to the catalogs of known sources. However, this method is not applicable to a new transient source. An example of such an event is an X-ray burst from Swift J1741.5−6548 (Negoro et al. 2013). MAXI detected a burst on 2012 December 25, and the position of the burst did not match with any known X-ray source. We reported the event as GRB 121225A at first (Ogawa et al. 2012). Two months later, Swift detected a previously unknown transient source (Krimm et al. 2013), and the position of the source was marginally consistent with the position of GRB 121225A. If a follow-up observation of GRB 121225A had been performed immediately

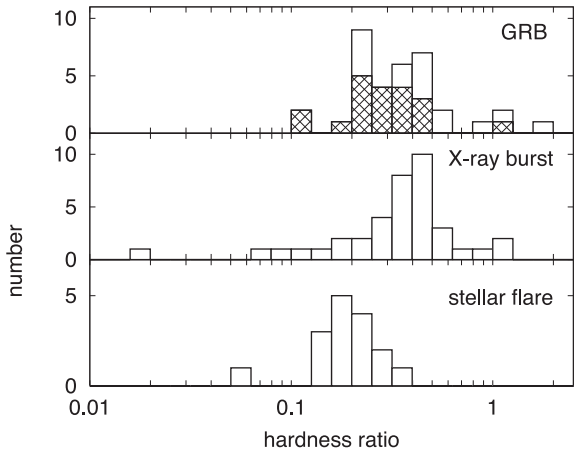

Fig. 12. The distribution of the hardness of GRBs, XRBs, and stellar flares observed with MAXI. The hardness is defined as the ratio of the photon flux in the 8–20 keV band to the 2–8 keV band. The hatched events in the top panel indicate "only MAXI" bursts.

after the MAXI detection, we would have found the counterpart. We learned the importance of immediate follow-up observations from this example.

There are possibilities for confusing XRBs from previously unknown sources like the example of Swift J1741.5−6548 in the MAXI GRB samples. In fact, HETE J1900.1−2455 was not known when HETE-2 detected the first XRB from this object (Vanderspek et al. 2005; Suzuki et al. 2007). Although a persistent emission from the XRB source is expected, MAXI is often not sensitive enough to detect a weak persistent emission. Therefore it is desirable to carry out follow-up observations with a highly sensitive X-ray telescope to find a persistent emission of a MAXI transient event to distinguish GRBs from XRBs.

Unlike GRBs or XRBs, stellar flares have a longer timescale than one scan interval of MAXI. So they are usually observed for multiple scans. Therefore they are easy to distinguish from GRBs or XRBs. Weak stellar flares may be observed only at their peak due to the sensitivity limit of MAXI. However, the hardness distribution of stellar flares (figure 12) peaks at around the lowest end of the hardness distribution of "only MAXI." Therefore, we can distinguish the "only MAXI" events from stellar flares by both temporal and spectral information. We believe that unknown stellar flares are less likely to be confused in our MAXI GRB samples.

4 Conclusion

We selected bright transient events at high ($>|10^{\circ}|$) galactic latitudes from the MAXI/GSC data. We calculated the average energy flux and hardness of these events. The results show that the bursts observed only by MAXI ("only MAXI") tend to have soft spectra and relatively low flux, compared to GRBs simultaneously observed by other satellites ("simul.-GRBs").

In comparison with the GRBs observed by HETE-2/WXM, the average fluxes of MAXI bursts are lower than those of HETE-2, while the effective area of GSC is 3–6 times smaller than that of WXM. This better sensitivity of GSC comes from its low background, which is a benefit of the slit and collimator optics. From the distributions of the hardness, we found that "only MAXI" bursts have a similar distribution of XRFs observed by HETE-2/WXM.

Since most MAXI bursts do not have enough statistics to perform spectral analysis, we compared the measured hardness with the calculated hardness assuming the standard GRB spectral parameters. As a result, we found most of the "only MAXI" events have hardness < 0.4, which corresponds to $E_{\rm peak} < 20\,{\rm keV}$.

As of now, there is no "only MAXI" burst with known redshift. The $\log N$–$\log S$ slope of "only MAXI" bursts is close to $-3/2$, while "simul.-GRBs" show slopes shallower than $-3/2$. The difference of the slope of "only MAXI" GRBs suggests that they are intrinsically dim and distributed closer than "simul.-GRBs."

We looked into the possibility that there was a confusion of galactic transients with the MAXI GRBs. Since the distributions of the hardness of X-ray bursts and stellar flares overlap with those of MAXI GRBs, it is difficult to classify these transients solely by hardness. The above facts suggest that it is essential to carry out follow-up observations and find counterparts. Direct measurement of redshift distribution and/or identifying counterparts in other wavelengths are needed to unveil those events.

Acknowledgments

This research was partially supported by the Ministry of Education, Culture, Sports, Science and Technology (MEXT), Grant-in-Aid Nos. 19047001, 20041008, 20244015, 21340043, 23740147, 24684015, 24740186, and Global-COE from MEXT "Nanoscience and Quantum Physics."

References

Band, D., et al. 1993, ApJ, 413, 281
Barthelmy, S. D., et al. 2005, Space Sci. Rev., 120, 143
Bhat, P. N., Chaplin, V., Connaughton, V., & Meegan, C. 2010, GCN Circ., 10745
Briggs, M. S. 2009, GCN Circ., 9957
Butler, N. R., Bloom, J. S., & Poznanski, D. 2010, ApJ, 711, 495
Cenko, S. B., Prochaska, J. X., Cucchiara, A., Perley, D. A., & Bloom, J. S. 2011, GCN Circ., 11736
Chen, H.-W., Helsby, J., Shectman, S., Thompson, I., & Crane, J. 2009, GCN Circ., 10038

D'Alessio, V., Piro, L., & Rossi, E. M. 2006, A&A, 460, 653
Fynbo, J. P. U., et al. 2012, GCN Circ., 14120
Fynbo, J. P. U., Malesani, D., Jakobsson, P., & D'Elia, V. 2009, GCN Circ., 9947
Golenetskii, S., et al. 2009a, GCN Circ., 10189
Golenetskii, S., et al. 2009b, GCN Circ., 9861
Golenetskii, S., et al. 2011, GCN Circ., 11722
Golenetskii, S., et al. 2012a, GCN Circ., 13446
Golenetskii, S., et al. 2012b, GCN Circ., 13295
Golenetskii, S., et al. 2012c, GCN Circ., 13351
Golenetskii, S., et al. 2013, GCN Circ., 14135
Gotz, D., Mereghetti, S., Bozzo, E., Ferrigno, C., Gibaud, L., & Borkowski, J. 2012, GCN Circ., 13434
Gotz, D., Mereghetti, S., Paizis, A., Bozzo, E., Gibaud, L., Ferrigno, C., Beck, M., & Borkowski, J. 2009, GCN Circ., 10298
Granot, J., Ramirez-Ruiz, E., & Perna, R. 2005, ApJ, 630, 1003
Gruber, D. 2009, GCN Circ., 10187
Gruber, D., & Pelassa, V. 2012, GCN Circ., 13437
Grupe, D., et al. 2009, GCN Circ., 9935
Heise, J., Zand, J. I., Kippen, R. M., & Woods, P. M. 2001, in Gamma-ray Bursts in the Afterglow Era, ed. E. Costa et al. (New York: Springer), 16
Kaneko, Y., Preece, R. D., Briggs, M. S., Paciesas, W. S., Meegan, C. A., & Band, D. L. 2006, ApJS, 166, 298
Krimm, H. A., et al. 2013, Astronomer's Telegram, 4902
Lamb, D. Q., Donaghy, T. Q., & Graziani, C. 2005, ApJ, 620, 355
Lien, A. Y., Sakamoto, T., Gehrels, N., Palmer, D., Barthelmy, S. D., Graziani, C., & Cannizzo, J. K. 2014, Abstract, Am. Astron. Soc. HEAD 14th Meeting, 352.06
Mangano, V., et al. 2010, GCN Circ., 11135
Maselli, A., et al. 2012, GCN Circ., 14045
Matsuoka, M., et al. 2009, PASJ, 61, 999
McGlynn, S. 2012, GCN Circ., 13741
Meegan, C., et al. 2009, ApJ, 702, 791
Meegan, C. A., Fishman, G. J., Wilson, R. B., Paciesas, W. S., Pendleton, G. N., Horack, J. M., Brock, M. N., & Kouveliotou, C. 1992, Nature, 355, 143
Mészáros, P., Ramirez-Ruiz, E., Rees, M. J., & Zhang, B. 2002, ApJ, 578, 812
Mihara, T., et al. 2011, PASJ, 63, S623
Morii, M., Sugimori, K., & Kawai, N. 2011, Physica E, 43, 692
Negoro, H., et al. 2013, Astronomer's Telegram, 4911
Ogawa, Y., et al. 2012, GCN Circ., 14100
Ohmori, N., et al. 2009, GCN Circ., 9900
Qin, S.-F., Liang, E.-W., Lu, R.-J., Wei, J.-Y., & Zhang, S.-N. 2010, MNRAS, 406, 558
Rau, A. 2009, GCN Circ., 9850
Ricker, G. R., et al. 2003, in AIP Conf. Ser., 662, Gamma-Ray Burst and Afterglow Astronomy 2001: A Workshop Celebrating the First Year of the HETE Mission, ed. G. R. Ricker & R. K. Vanderspek (New York: AIP), 3
Sakamoto, T. 2004, PhD thesis, Tokyo Institute of Technology
Sakamoto, T., et al. 2004, ApJ, 602, 875
Sakamoto, T., et al. 2005, ApJ, 629, 311
Sakamoto, T., et al. 2006, ApJ, 636, L73
Sakamoto, T., et al. 2008, ApJ, 679, 570
Sakamoto, T., et al. 2011, ApJS, 195, 2
Serino, M., et al. 2011, PASJ, 63, S1035
Shirasaki, Y., et al. 2003, PASJ, 55, 1033
Soderberg, A. M., et al. 2004, ApJ, 606, 994
Soderberg, A. M., et al. 2007, ApJ, 661, 982
Sonbas, E., D'Elia, V., Kennea, J. A., Krimm, H. A., Sakamoto, T., & Siegel, M. H. 2012, GCN Circ., 14115
Stern, B. E., Atteia, J.-L., & Hurley, K. 2002, ApJ, 578, 304
Strohmayer, T. E., Fenimore, E. E., Murakami, T., & Yoshida, A. 1998, ApJ, 500, 873
Sugizaki, M., et al. 2011, PASJ, 63, S635
Suwa, F., Negoro, H., Ozawa, H., Serino, M., & the MAXI team 2010, in The First Year of MAXI: Monitoring Variable X-ray Sources (Wako, Saitama: RIKEN), 63
Suzuki, M., et al. 2007, PASJ, 59, 263
Suzuki, M., & the MAXI team 2009, in Proc. Astrophysics with All-Sky X-Ray Observations: 3rd international MAXI workshop, JAXA-SP-08-014E (Tokyo: JAXA), 224
Tam, P. H. T., Li, K. L., & Kong, A. K. H. 2012, GCN Circ., 13444
Tanvir, N. R., Wiersema, K., Levan, A. J., Fox, D., Fruchter, A., & Krogsrud, D. 2012, GCN Circ., 13441
Tomida, H., et al. 2011, PASJ, 63, 397
Tsunemi, H., Tomida, H., Katayama, H., Kimura, M., Daikyuji, A., Miyaguchi, K., Maeda, K., & the MAXI Team 2010, PASJ, 62, 1371
van der Horst, A. J., & Camero-Arranz, A. 2011, GCN Circ., 12013
Vanderspek, R., Morgan, E., Crew, G., Graziani, C., & Suzuki, M. 2005, Astronomer's Telegram, 516
Virgili, F. J., Zhang, B., Nagamine, K., & Choi, J.-H. 2011, MNRAS, 417, 3025
Wanderman, D., & Piran, T. 2010, MNRAS, 406, 1944
Wiersema, K., et al. 2012, MNRAS, 426, 2
Yamaoka, K., et al. 2009, PASJ, 61, S35
Yamazaki, R., Ioka, K., & Nakamura, T. 2002, ApJ, 571, L31
Zhang, B., & Mészáros, P. 2002, ApJ, 581, 1236